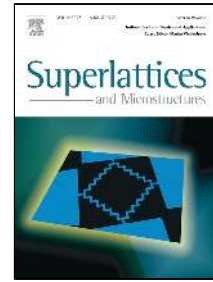


Accepted Manuscript

Synergistic effect of temperature and point defect on the mechanical properties of single layer and bi-layer graphene



Sanghamitra Debroy, V.Pavan Kumar, K.Vijaya Sekhar, Swati.G. Acharyya, Amit Acharyya

PII: S0749-6036(17)31079-0

DOI: 10.1016/j.spmi.2017.08.040

Reference: YSPMI 5215

To appear in: *Superlattices and Microstructures*

Received Date: 02 May 2017

Revised Date: 11 August 2017

Accepted Date: 23 August 2017

Please cite this article as: Sanghamitra Debroy, V.Pavan Kumar, K.Vijaya Sekhar, Swati.G. Acharyya, Amit Acharyya, Synergistic effect of temperature and point defect on the mechanical properties of single layer and bi-layer graphene, *Superlattices and Microstructures* (2017), doi: 10.1016/j.spmi.2017.08.040

This is a PDF file of an unedited manuscript that has been accepted for publication. As a service to our customers we are providing this early version of the manuscript. The manuscript will undergo copyediting, typesetting, and review of the resulting proof before it is published in its final form. Please note that during the production process errors may be discovered which could affect the content, and all legal disclaimers that apply to the journal pertain.

Synergistic effect of temperature and point defect on the mechanical properties of single layer and bi-layer graphene

Sanghamitra Debroy¹, V. Pavan Kumar¹, K. Vijaya Sekhar², Swati G.Acharyya^{2*},
Amit Acharyya¹

¹Department of Electrical Engineering, Indian Institute of Technology, Hyderabad, India

²School of Engineering Sciences and Technology, University of Hyderabad, India

The present study reports a comprehensive molecular dynamics simulation of the effect of a) temperature (300-1073 K at intervals of every 100 K) and b) point defect on the mechanical behaviour of single (armchair and zigzag direction) and bilayer layer graphene (AA and AB stacking). Adaptive intermolecular reactive bond order (AIREBO) potential function was used to describe the many-body short-range interatomic interactions for the single layer graphene sheet. Moreover, Lennard Jones model was considered for bilayer graphene to incorporate the van der Waals interactions among the interlayers of graphene. The effect of temperature on the strain energy of single layer and bilayer graphene was studied in order to understand the difference in mechanical behaviour of the two systems. The strength of the pristine single layer graphene was found to be higher as compared to bilayer AA stacked graphene at all temperatures. It was observed at 1073 K and in the presence of vacancy defect the strength for single layer armchair sheet falls by 30% and for bilayer armchair sheet by 33% as compared to the pristine sheets at 300 K. The AB stacked graphene sheet was found to have a two-step rupture process. The strength of pristine AB sheet was found to decrease by 22 % on increase of temperature from 300K to 1073K.

Keywords: Single layer graphene sheet, AA and AB stacked graphene sheet, Molecular Dynamics simulation, Temperature effect, Point defect effect.

1. Introduction

Graphene has attracted enormous interest among the researchers since its discovery [1-23], due to its amazing mechanical and electrical properties. This makes it a potential material for a wide range of applications. Experiments on the mechanical behaviour of graphene are restricted owing to the practical complications in designing experiments at nanoscale [3, 15–16]. Therefore, atomistic methods such as MD have been extensively used to study the mechanics of graphene [11, 17–23].

However, previous studies have focussed on the mechanical properties of single layer graphene (SLG) [11, 19-23] and little has been explored about the mechanical properties of bilayer graphene (BLG) [24-26] and its variation with temperature. Since defects play a key role in determining the mechanical properties of graphene [27-30], understanding the variation of strength of the BLG with temperature both in pristine condition as well as in presence of the defects (e.g. vacancies) is a prerequisite for its successful application at higher temperatures. Different experimental methods reported for synthesis of graphene show that generally the final product contains a mix of single layer and bilayer graphene [31-32]. Moreover, in most of the large scale techniques, it is common to find few layered graphene (up to ten layers) in the final products [33-34]. However, no literature exists to the best of the author's knowledge in this direction. A detailed and systematic investigation has been carried out in this paper at various temperatures (300-1073K, at intervals of 100 K) and in presence of point defect to determine the strength of SLG and BLG both in zigzag and armchair direction and for different stacking conditions (AA and AB for bilayer graphene).

2. Simulation Model and Method

The primary objective of the present study is to understand the effect of temperature on the strength of single-crystal graphene, which is an uprising material especially for electronic applications. Grain boundaries (GB) in graphene decreases both the electrical and mechanical quality of graphene films [35-36] and hence several efforts have been made towards enlarging the sizes of single-crystal graphene (single layer and bilayer) domains experimentally to millimetre and even centimetre scale [37-43]. Graphene single crystals exert great advantages over polycrystalline graphene especially in high mobility graphene-based nano-electronics, due to the absence of GBs. The GBs act as defects resulting in higher surface chemical activity, [44] and changes the sp^2 -bonding nature of graphene. GBs has been found to be detrimental to the carrier transport properties as they act as the scattering centres for charge transport. Hexagonal graphene single crystals grown on a Cu surface greatly decreases the defect density, resulting in a largely improved FET performance with carrier mobility higher than $1900 \text{ cm}^2 \text{ V}^{-1} \text{ s}^{-1}$ [45].

Here, Molecular dynamics (MD) simulations were carried out using LAMMPS [46] with the AIREBO potential [47] for the analysis of single and bilayer pristine graphene sheet at temperatures between 300K – 1073 K at the intervals of 100 K and also in the presence of vacancy defect as detailed in Table 1. The aim of this simulation is to calculate the force acting

on individual atoms via atom-atom interaction potential and further calculate atomic trajectory, acceleration & velocity using Newtonian -mechanics equations. These MD simulations have been extensively used by researchers to analyse deformation nature at non level in different materials. The prime factor is to identify the ideal atomic potential function for accurate results. The AIREBO potential primarily has three sub potentials, which are the REBO, Lennard–Jones, and torsional potentials. The REBO potential provides the energy stored in atomic bonds, while Lennard–Jones potential considers the non-bonded interactions between atoms, and the torsional potential includes the energy from torsional interactions between atoms. Brenner and co-workers provided the AIREBO parameters for the carbon-hydrogen system, with two cut off distances of C-C bonding (D_1 and D_2) as 1.7 Å and 2.0 Å. Authors of [48] have stated that there exist some differences (~20%) in Young’s modulus of graphene obtained by DFT calculations as compared to MD simulations. The differences arise due to the fact that the study of the elastic deformation of finite graphene sheets by DFT discussed in [48] has been based on Brenner potential whereas the present study has been based on AIREBO potential. Brenner potential does not consider the dispersion and repulsion terms and hence is less suitable for a system having significant intermolecular interactions. AIREBO potential on the other hand has been shown to exactly capture the bond-bond interaction between carbon atoms as well as bond breaking and bond re-forming [49]. A cut-off function has been also used in the simulations carried on here in order to suppress the high bond forces that can arise with nonphysical explanations. The cut-off parameter is set to be 2.0 Å for the REBO part of the potential, as suggested in ref [49], which is an acceptable approximation for the near fracture regime. The MD calculations indicate that the Young’s modulus Y is 1.01 ± 0.03 TPa that matches to the experimental results of Lee et al [6].

The graphene sample used in this simulation is 5 nm x 5 nm sheet with each time step equivalent to 1 ps & consists of 1008 carbon atoms for single layer and 2016 carbon atoms for bilayer model with interlayer distance of 3.4 Å. In the present study, velocity-verlet time integrating scheme was applied to graphene with a time step of 0.0005 ps and the system was maintained at equilibrium for 30 ps to ensure that equilibrium thermodynamic state was reached where the temperature was controlled by using Nose-Hoover thermostat. Uniaxial tensile loading was subsequently applied strain rate of 0.001/ps. The results were also validated with that of literature [6, 10, 21, 24-25, 53-55] which confirmed that the graphene sheet was in the state of thermodynamic equilibrium before the onset of tensile testing using MD simulation.

The interlayer cohesion in bilayer sheet was maintained by van der Waals force and is characterized by the 12-6 Lennard-Jones potential [50]:

$$V(r) = 4\epsilon \left[\left(\frac{\sigma}{r} \right)^{12} - \left(\frac{\sigma}{r} \right)^6 \right] \dots \dots \dots (1)$$

r is the distance between a pair of atoms while ϵ i.e. the depth of the potential well is = 2.84 meV and σ , the finite distance for zero inter-particle potential which here is = 0.340 nm. The directions in a bilayer sheet of graphene, i.e., AA stacked graphene has either armchair-armchair type orientation or zigzag-zigzag type and AB stacked graphene sheet has armchair orientation as one layer and zigzag in the other layer [51, 52].

The convention for direction as used in the present study for loading of graphene sheet is shown in Figure 1.

Table 1: Graphene test conditions with varying orientations and defect morphology

Structure		Defect type	Orientations	Test condition of graphene sheet
Single Layer (SLG)		<ul style="list-style-type: none"> • Pristine (Pr) • Vacancy (V) 	<ul style="list-style-type: none"> • Armchair (A) 	1. Pristine (SLG-Pr-A)
				2. Vacancy (SLG-V-A)
			<ul style="list-style-type: none"> • Zigzag (Z) 	3. Pristine (SLG-Pr-Z)
				4. Vacancy (SLG-V-Z)
Bi-Layer (BLG)	AA			5. Pristine (BLG-AA-Pr-A)
				6. Vacancy (BLG-AA-V-A)
	AB			7. Pristine (BLG-AA-Pr-Z)
				8. Vacancy (BLG-AA-V-Z)
		9. Pristine (BLG-AB-Pr)		
		10. Vacancy (BLG-AB-V)		

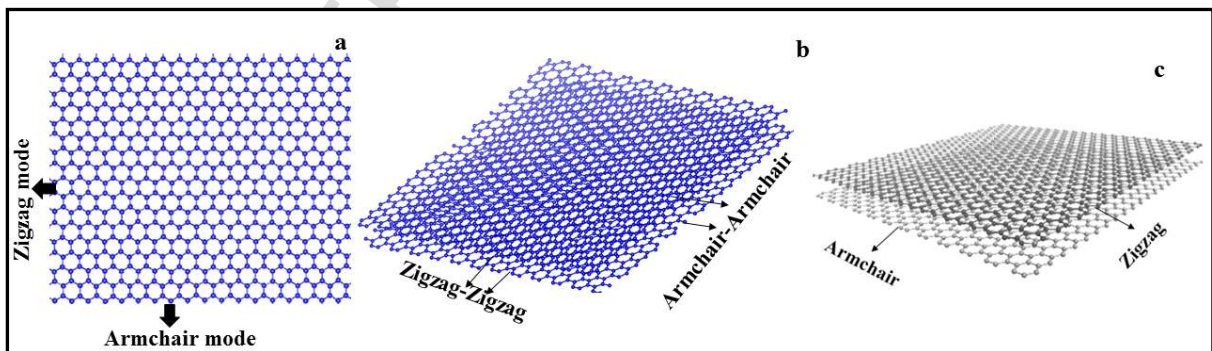


Figure 1 Conventions used for (a) single layer graphene sheet, (b) AA stacked bilayer graphene model and (c) AB stacked graphene sheet.

3. Results and Discussion

3.1. Validation of the models

The models used for the present study has been validated by comparing the fracture stress and strain with that of the literature [6, 10, 21, 24-25, 53-55]. The nominal fracture strengths of the SLG were determined to be 90 GPa at 0.14 and 102 GPa at 0.22 fracture strain, respectively for armchair and zigzag mode, which is in the range of reported values [6, 10, 53-55]. The tensile strength variation of armchair pristine sheet with increasing temperature were also found to be at par with the literature [11, 21], thereby validating the present model. The stress and strain at fracture for the AA stacked armchair and zigzag pristine BLG sheet was found to be 88 GPa at 0.14 and 100 GPa at 0.2 strain respectively at room temperature, which was found to be consistent with the previously reported values [24-25].

3.1.1 Effect of Temperature on the mechanical properties of pristine single layer and bilayer (AA stacked) graphene sheet

The stress-strain plots indicating the mechanical behaviour of the single and bi-layer graphene at various temperatures ranging from 300K-1073 K at the intervals of 100 K is shown in the Figure 2. The ultimate tensile strength of single and bi-layer graphene in pristine condition and in the presence of vacancy at different temperatures is given in Table 2. The fracture strength and fracture strain decreases significantly with the increase in temperature both for single and bi-layer graphene. The fracture strength at 1073 K for single layer armchair and zigzag graphene sheet is 23% and 25% less respectively compared to that at room temperature whereas for bilayer AA armchair and zigzag graphene sheet the reduction of strength is nearly 25% and 28%.

Table 2: Tensile strength of Graphene at different temperatures with varying orientations and defect

Sl. No	Test conditions	Ultimate Tensile strength (GPa) at different temperatures							
		300K	400K	500K	600K	700K	800K	900K	1073K
1.	SLG-Pr-A	90	86.2	82.5	81	80.6	77.1	74.3	69
2.	SLG-Pr-Z	102	96	94	90.6	88	85.8	81	77
3.	SLG-V-A	76	74.5	72	70.3	68.5	67	65	63
4.	SLG-V-Z	82	80	79.1	77.9	76.5	75.2	73	70
5.	BLG-AA-Pr-A	88	87.1	86	84	79	75.2	73	66
6.	BLG-AA-Pr-Z	100	97	93.5	90	85	83.1	77.2	72
7.	BLG-AA-V-A	73	71.6	69	67.9	65	62.3	61.4	59
8.	BLG-AA-V-Z	75	74	73.4	72.9	71.7	71.1	70	69
9.	BLG-AB-Pr	87	85.6	82.6	79.3	76.2	74.9	72.6	68
10.	BLG-AB-V	72	69.1	68.3	66.6	64.6	62.9	59.7	55

The tensile strength of BLG is always less than the corresponding SLG sheet (3-7%) and the difference increases with the rise in temperature (from 2GPa at 300K to ~5GPa at 1073K) which is graphically depicted in Fig. 2- I & II. Tensile strength of SLG was found to be higher by 4% in armchair & 6.4% zigzag direction at 1073K as compared to BLG with AA stacking. The pristine graphene sheets in both cases fail by homogeneous nucleation of defects followed by growth and coalescence of defects.

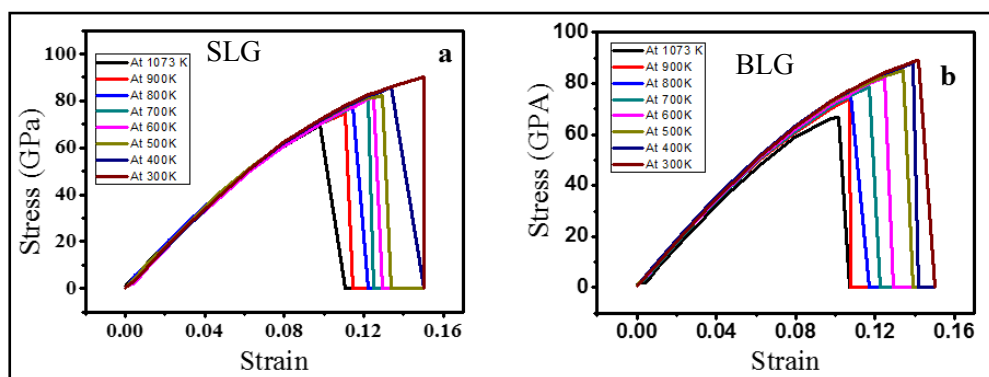


Figure 2-I: Nominal Stress vs. Strain plot for pristine sheet in Armchair direction for (a) SLG and (b) BLG – AA stacking.

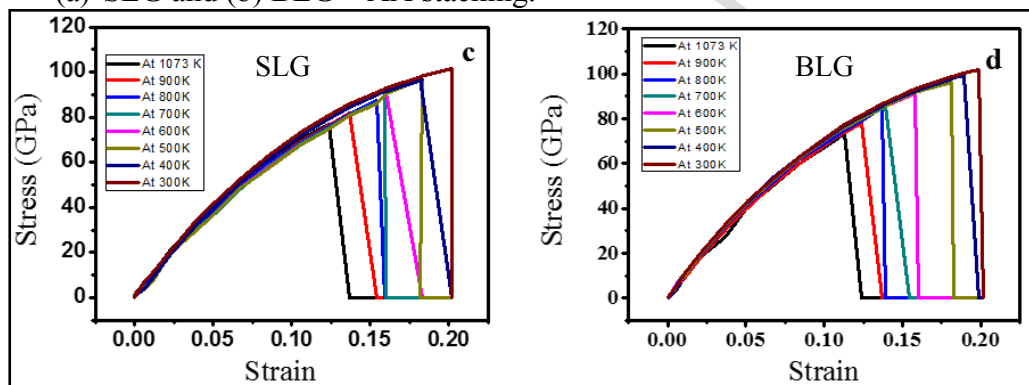


Figure 2-II: Nominal Stress vs. Strain plot for pristine sheet in Zigzag direction for (c) SLG and (d) BLG – AA stacking.

3.1.2 Critical strain energy of the carbon atoms at fracture: correlation with the fracture behaviour of single and bilayer graphene (AA stacking)

As highlighted in the previous sections, the UTS for SLG is greater than BLG by a minimum value of 2GPa. To understand the reason behind the difference in UTS of SLG and BLG, the strain energy of the atoms of SLG and BLG was determined at different strain levels. Figure 3 shows the plot of strain energy per atom vs. strain for SLG and BLG at room temperature and at 1073 K. The strain energy is determined as the difference in total energy per atom of the strained and unstrained graphene sheets on application of uniaxial tensile loading using the AIREBO potential function. As shown in Figure 3, the critical strain energy before fracture for

the atoms of SLG is much higher than that of BLG. Hence, the presence of van der Waals force in between the graphene layers in BLG have an effect on the nature and magnitude of the interatomic bonds in graphene and affects the critical strain energy of the carbon atoms.

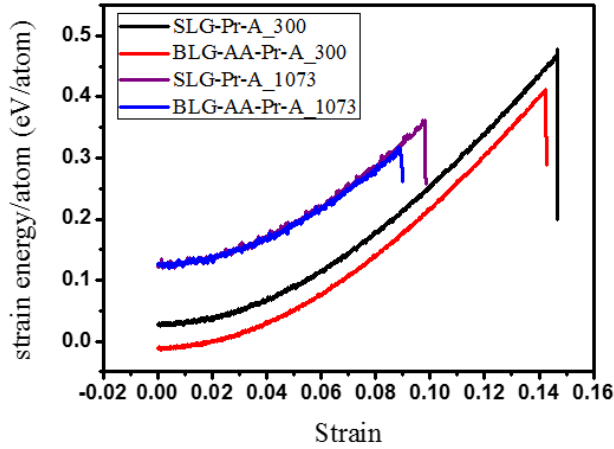


Figure 3: Strain energy per atom of the single and AA stacked bilayer graphene sheet oriented in armchair direction at 300 K and 1073 K

The decrease in strength of bilayer sheet as compared to single layer sheet is consistent with the total energy calculation using AIREBO potential [47], which is given as:

$$E = \frac{1}{2} \sum_i \sum_{j \neq i} [E_{ij}^{REBO} + E_{ij}^{LJ} + \sum_{k \neq i,j} \sum_{l \neq i,j,k} E_{kijl}^{tors}] \dots \dots \dots (2)$$

Where E_{ij}^{REBO} represents the covalent bonding (REBO) interactions, E_{ij}^{LJ} represents the LJ terms, and E_{kijl}^{tors} represents the torsion interactions respectively. In our case E_{kijl}^{tors} is kept zero as only the covalent and interlayer cohesive forces are considered in the simulation and no torsional interactions are considered. The term E_{ij}^{REBO} that represents the covalent bonding (REBO potential) is given as:

$$E_{ij}^{REBO} = V_{ij}^R + b_{ij} V_{ij}^A \dots \dots \dots (3)$$

The functions V^R and V^A are pair-additive interactions that represent all interatomic repulsions (core-core, etc.) and attraction from valence electrons. The quantity r_{ij} is the distance between pairs of nearest-neighbour atoms i and j , and b_{ij} is a bond order between atoms i and j that is derivable from Huckel or similar level electronic structure theory. The repulsive term has the form:

$$V_{ij}^R = w_{ij}(r_{ij}) \left[1 + \frac{Q_{ij}}{r_{ij}} \right] A_{ij} e^{-\alpha_{ij} r_{ij}} \dots \dots \dots (4)$$

The attractive pair interaction is given as

$$V_{ij}^A = -w_{ij}(r_{ij}) \sum_{n=1}^3 B_{ij}^{(n)} e^{-\beta_{ij}^n r_{ij}} \dots \dots \dots (5)$$

The parameters $W_{ij}, Q_{ij}, A_{ij}, \alpha_{ij}, B_{ij}$ and β_{ij} are defined in [47]. For single layer graphene sheet the REBO potential function is valid i.e. equation (4) and (5) V_{ij}^R and V_{ij}^A are inserted in equation (3) and then E^{REBO} is inserted in equation (2). The rest of the terms are equal to zero. In case of the BLG sheet the intralayer carbon atoms are bonded through E^{REBO} that includes the functions V_{ij}^R and V_{ij}^A that represent all interatomic repulsions (core-core, etc.) and attraction from valence electrons respectively and the interlayer carbon bonds are defined through $V(r)$ that represents the interlayer cohesion maintained by van der Waals force was characterized by the 12-6 Lennard-Jones potential. Therefore inserting equations (4) and (5) in equation (3) in order to obtain E^{REBO} and then equation (3) and equation (1) are inserted in equation (2) in order to obtain the entire system energy vs. the interatomic distance. The values of all the parameter are adopted from Stuart et al. [47].

The entire system energy for both single and bi-layer graphene as a function of interatomic spacing is shown in Figure 4 (a). Figure 4 (b) shows the van der Waals forces acting in between the layers of bilayer graphene.

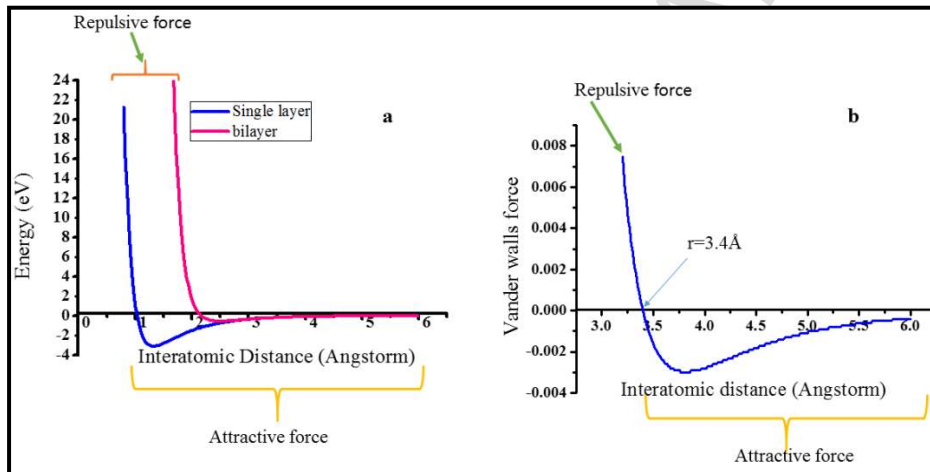


Figure 4 (a): Plot shows the attractive and repulsive pair terms as a function of the interatomic distance for single and bilayer graphene sheet and (b) van der Waals force between interlayer atoms.

As seen from Figure 4 (a), the attractive forces between the atoms in SLG are much higher as compared to that of BLG. Higher interatomic attractions leads to more stability and hence greater forces would be required to rupture the interatomic bonds, hence the UTS of SLG is higher compared to the BLG. In case of BLG, the interatomic interaction is influenced by the presence of van der Waals forces (as shown in Figure 4b) resulting in decrease in the strength of inter atomic bonds (in plane) and hence lower UTS.

3.1.3. Effect of temperature and fracture mechanism of AB stacked bilayer graphene sheet

AB-stacking system has attracted much attention, since it is stable as compared to the AA stacked BLG and is used in common graphene-based devices [51]. The effect of temperature on the stress-strain plot for the AB stacked pristine BLG sheet is shown in Figure 5.

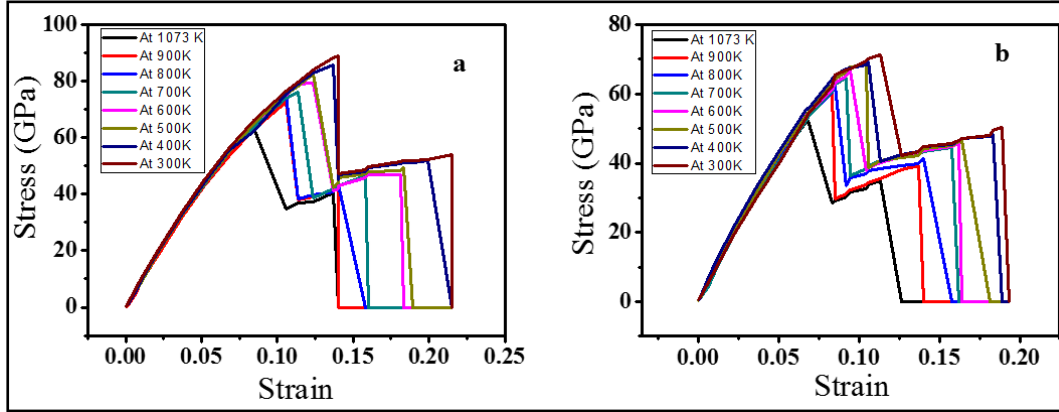


Fig. 5: Nominal Stress vs. Strain plot for AB stacked BLG sheet (a) Pristine & (b) Vacancy defect

In the case of AB stacked bilayer graphene sheet, the initial drop in strength for 300 K was observed at 0.14 strain where the strength of the sheet decreased from 87 GPa to an intermediate value of 40 GPa which is consistent with the published reports [25]. Figure 7 (a) indicates that at the strain of 0.14, the armchair constituent of the sheet failed. The zigzag constituent was still intact and continued to carry the external load on the sheet up to a stress value of 54 GPa following which the entire sheet failed. Increase of temperature to 1073K reduced the strength of the AB stacked bilayer sheet to 68 GPa at 1st rupture point and 42 GPa for the second rupture point which is 22% and 25 % less as compared to 300K. The result shows that temperature has a profound effect on the mechanical properties of AB stacked bilayer sheet.

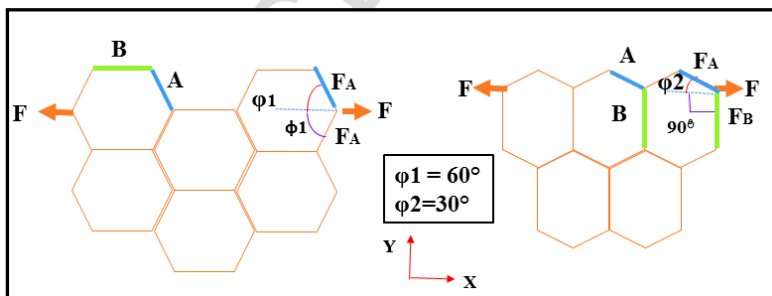


Figure 6: Graphene sheet with armchair and zigzag edges. A uniaxial tensile test in the armchair direction refers to the figure on the left and for zigzag direction it is the figure on the right.

Fracture occurred in the AB stacked bilayer graphene sheet by a step-by-step rupture process due to the presence of mixed chirality as shown in Figure 1(c) and was independent of loading direction. Applying classical mechanics theory, it can be explained that when uniaxial tensile force F is applied to the armchair and zigzag direction of a graphene sheet at equilibrium (Figure 6) the components of force in armchair and zigzag direction are as follows:

Armchair Direction

$$F_{arm} = F_A \cos \varphi_1 + F_A \cos \varphi_1 = 2F_A \cos \varphi_1 \dots \dots \dots (6)$$

Zigzag Direction

$$F_{zig} = F_A \cos \varphi_2 + F_B \cos 90^\circ = F_A \cos \varphi_2 \dots \dots \dots (7)$$

Inserting $\varphi_1 = 60^\circ$ for armchair direction and $\varphi_2 = 30^\circ$ for zigzag direction, we obtain:

$$F_A = 1.15 F_{zig} \dots \dots \dots (8)$$

Using the above equation (8), it was found that for the fracture to occur the critical stress for Armchair: Zigzag = 1:1.15 and therefore the fracture strength of zigzag graphene is higher than that of its armchair counterpart.

The fracture strain obtained by using the homogeneous deformation Cauchy-Born rule [56] also explains the two step rupture process that is given as:

$$\varepsilon_{bb}(\chi) = 2(\partial l/l)_{bb} [(1 - \nu) + (1 + \nu) \cos 2\chi]^{-1} \dots \dots \dots (9)$$

where ε_{bb} is the brittle breaking strain or fracture strain, $(\partial l/l)_{bb}$ is the individual bond elongation at the brittle breaking point, ν is the Poisson's ratio, and χ is the chiral angle which is equal to 0° for the armchair case and 30° for the zigzag case, it can be estimated that ε_{bb} , armchair:zigzag = 0.66:1.00. Therefore from fracture strength and fracture strain concepts it is noticeable that the fracture initially occurs in the armchair component followed by the zigzag counterpart leading to a two-step rupture process as shown in Figure 7.

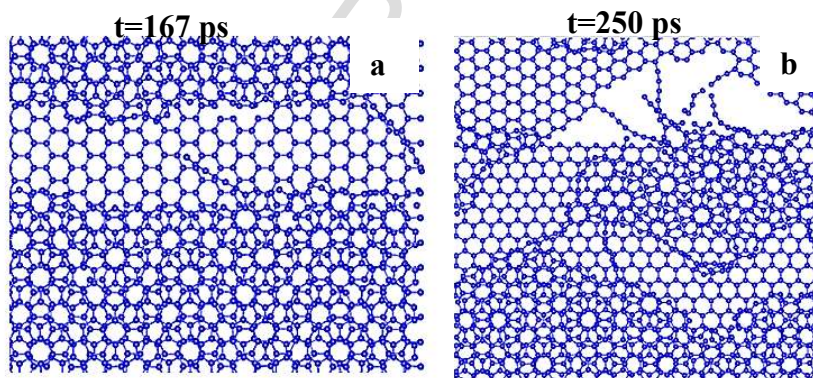


Figure 7(a): Failure of armchair component in the AB stacked sheet and (b) Failure of both the armchair and the zigzag component in the AB stacked bilayer sheet

3.2.1 Effect of temperature and vacancy defect on single and bilayer sheet

The fracture strength of single and AA stacked bilayer graphene sheet in the presence of vacancy was evaluated under uniaxial tensile load along the armchair and zigzag direction in the temperature range of 300K–1073 K. The simulation model has one vacancy placed in the centre of the sheet for the single layer. For bilayer graphene, the vacancy is inserted in the centre of only one layer as shown in Figure 8.

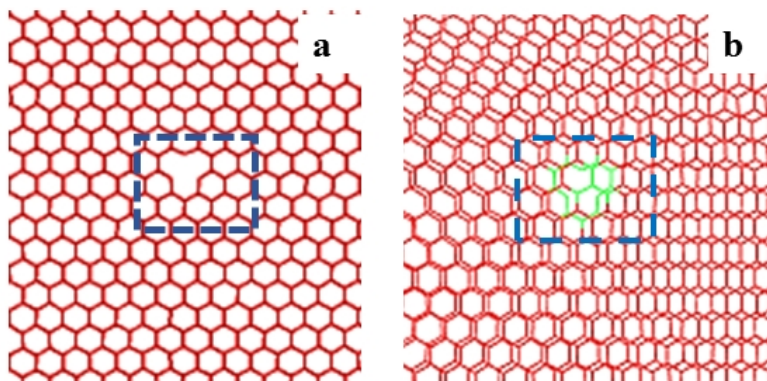


Figure 8: Graphene sheet with vacancy defect for (a) SLG sheet and (b) BLG sheet.

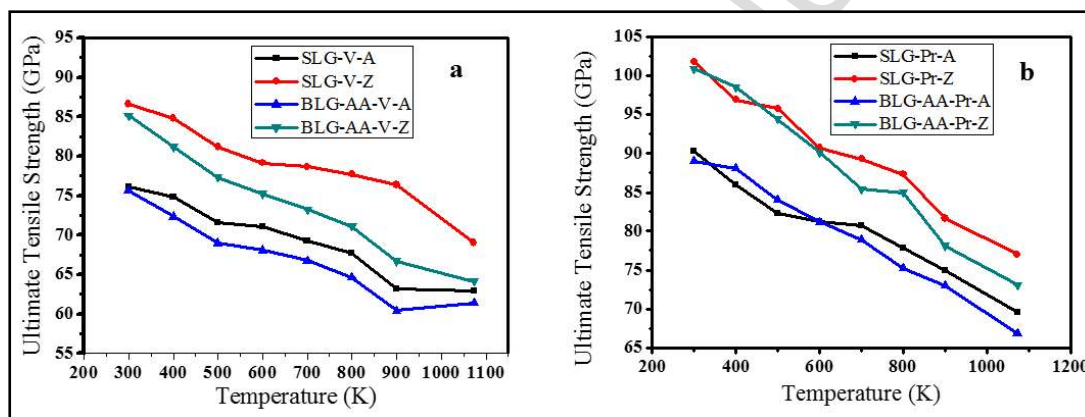


Figure 9 (a): Variation of fracture strength of graphene sheet w.r.t. temperature for SLG & BLG in Armchair & Zigzag direction (a) vacancy defect & (b) pristine condition.

It was observed that one missing carbon atom reduced the strength of armchair and zigzag single layer graphene sheet by 15% and 20% at 300 K temperature respectively, as compared to the pristine sheet which is at par with literature [23] whereas for bilayer the reduction in strength was 17% in armchair and 25% in zigzag direction at 300 K temperature. As evident from Figure 9 (a), the severity increases with rise temperature where at 1073 K the strength falls for single layer armchair sheet by 30% and bilayer armchair sheet by 33% as compared to pristine sheets at 300K. Therefore, in atomic scale defect such as vacancy plays a critical role in dictating the mechanical performance of graphene.

3.2.2. Vacancy defect in AB bilayer sheet

The effect of temperature on the stress-strain behaviour for AB stacked pristine bilayer graphene sheet is shown in Figure 5 (b). The strength of AB stacked bilayer sheet with a vacancy reduced by 24% for the first rupture point and 32 % for the second rupture step for the increase in temperature from 300 K to 1073 K. Hence the mechanical properties of AB stacked bilayer sheet decreases drastically by the synergistic effect of temperature and defect.

4. Conclusion

The effect of temperature and defects on the mechanical properties of single and bilayer graphene were investigated by performing uniaxial tensile test in armchair and zigzag direction and also for differently stacked bilayer graphene. The findings of the study are summarised as follows:

1. The strength of the SLG is always higher compared to that of the BLG by 2-5 GPa.
2. The tensile strength for both single and bi-layer graphene reduces with increase in the temperature from 300K-1073 K. The reduction is $\sim 23 \pm 2$ % for single layer graphene and 25 ± 3 % for bilayer graphene (AA and AB stacked). This is due to the decrease in binding energy between carbon atoms and the elongation of C-C bond-length with rise in temperature.
3. In presence of the defect, while increasing the temperature from 300K to 1073 K, the strength of both single and bi-layer graphene falls upto 33%, with severity of defect being more pronounced at lower temperatures.
4. The failure of the pristine graphene sheets in all cases occurred by homogeneous nucleation of defects followed by growth and coalescence of defects.
5. AB stacked graphene sheet (both in pristine & defective) was found to have a two-step failure process. The ultimate tensile strength of AB graphene at 1073 K was found about 23% less than that of 300 K.

Acknowledgement

The authors would like to thank Department of Science and Technology for the INSPIRE fellowship provided to Sanghamitra Debroy (Grant: IF131049) and University Grants Commission (UGC), Government of India, Rajiv Gandhi National Fellowship (grant RGNF201517SCAND26105) PhD fellowship to K. VijayaSekhar which helped in successful completion of the study.

References

1. K.S. Novoselov, A.K. Geim, S.V. Morozov, D. Jiang, Y. Zhang, S.V. Dubonos, et al., Electric field effect in atomically thin carbon films, *Science* 306, (2004), 666-669, doi: 10.1126/science.1102896
2. C. H. Yeh, Y. W. Lain, Y. C. Chiu, C. H. Liao, D. R. Moyano, S. S. Hsu, and P. W. Chiu, Gigahertz flexible graphene transistors for microwave integrated circuits, *ACS Nano* 8 (8), (2014), 7663, doi: 10.1021/nl5036087.
3. K. S. Novoselov, V. I. Fal'ko, L. Colombo, P. R. Gellert, M. G. Schwab, K. Kim, A roadmap for graphene, *Nature* 490, (2012), 192, doi:10.1038/nature11458.
4. A. V. Krasheninnikov, and F. Banhart, Engineering of nanostructured carbon materials with electron or ion beams, *Nature Materials* 6, (2007), 723, doi:10.1038/nmat1996
5. J. Heo, K. E. Byun, J. Lee, H. J. Chung, S. Jeon, S. Park et al., Graphene and Thin-Film Semiconductor Heterojunction Transistors Integrated on Wafer Scale for Low-Power Electronics, *Nano Lett.*, 13 (12), (2013), 5967, doi: 10.1021/nl403142v.
6. C. Lee, X. Wei, J. W. Kysar, and J. Hone, Measurement of the Elastic Properties and Intrinsic Strength of Monolayer Graphene, *Science* 321, (2008), 385, doi: 10.1126/science.1157996.
7. I. W. Frank, D. M. Tanenbaum, A. M. van der Zande, and P. L. McEuen, Mechanical properties of suspended graphene sheets, *J. Vac. Sci. Technol. B* 25, (2007), 2558, DOI: 10.1116/1.2789446.
8. F. Liu, P. Ming, and J. Li, *Ab initio* calculation of ideal strength and phonon instability of graphene under tension, *Phys. Rev. B* 76, (2007), 064120, DOI: <https://doi.org/10.1103/PhysRevB.76.064120>
9. A.C. Ferrari, J.C. Meyer, V. Scardaci, C. Casiraghi, M. Lazzeri, F. Mauri, et al., Raman Spectrum of Graphene and Graphene Layers, *Phys. Rev. Lett.* 97, (2006), 187401. <http://dx.doi.org/10.1103/PhysRevLett.97.187401>.
10. H. Zhao, K. Min, and N. R. Aluru, Size and Chirality Dependent Elastic Properties of Graphene Nanoribbons under Uniaxial Tension, *Nano Lett.* 9, (2009), 3012, DOI: 10.1021/nl901448z
11. H. Zhao and N. R. Aluru, Temperature and strain-rate dependent fracture strength of graphene, *J. Appl. Phys.* 108, (2010), 064321, doi: <http://dx.doi.org/10.1063/1.3488620>
12. A. Sakhaee-Pour, Elastic properties of single-layered graphene sheet, *Solid State Commun.* 149, (2009), 91, <http://dx.doi.org/10.1016/j.ssc.2008.09.050>.
13. M.Q. Le, R.C. Batra, Crack propagation in pre-strained single layer graphene sheets, *Comput. Mater. Sci.* 84, (2014), 238–243, <http://dx.doi.org/10.1016/j.commatsci.2013.12.007>.
14. Sanghamitra Debroy, V. Pavan Kumar Miriyala, K. VijayaSekhar, Swati Ghosh Acharyya, Amit Acharyya, Graphene heals thy cracks, *Comput. Mater. Sci.* 109, (2015), 84, <http://dx.doi.org/10.1016/j.commatsci.2015.05.025>.
15. F. Banhart, J. Kotakoski, and A. V. Krasheninnikov, Structural Defects in Graphene, *ACS Nano*, 5(1), (2011), 26, DOI: 10.1021/nl102598m
16. L. Gao, G. X. Ni, Y. P. Liu, B. Liu, A. H. C. Neto and K. P. Loh, Face-to-face transfer of wafer-scale graphene films, *Nature*, 505, (2014), 190, doi:10.1038/nature12763.
17. C. Carpenter, D. Maroudas, and A. Ramasubramaniam, Mechanical properties of irradiated single-layer graphene, *Appl. Phys. Lett.*, 103(1), (2013), 013102, doi: <http://dx.doi.org/10.1063/1.4813010>.

18. L. Xu, N. Wei, and Y. Zheng, Mechanical properties of highly defective graphene: from brittle rupture to ductile fracture, *Nanotechnology*, 24(50), (2013), 505703, <https://doi.org/10.1088/0957-4484/24/50/505703>.
19. C. Hou, H. Wang, Q. Zhang, Y. Li and M. Zhu, Highly Conductive, Flexible, and Compressible All-Graphene Passive Electronic Skin for Sensing Human Touch, *Adv. Mater.* 26 (29), (2014), 5018-5024, <http://dx.doi.org/10.1002/adma.201401367>.
20. C.H. Wong and V. Vijayaraghavan, Nanomechanics of free form and water submerged single layer graphene sheet under axial tension by using molecular dynamics simulation, *Mater. Sci. Eng. A* 556, (2012), 420-428, <http://dx.doi.org/10.1016/j.msea.2012.07.008>.
21. M. A. N. Dewapriya and R. K. N. D. Rajapaske, Molecular Dynamics Simulations and Continuum Modeling of Temperature and Strain Rate Dependent Fracture Strength of Graphene With Vacancy Defects, *J. Appl. Mech.* 81(8), (2014), 081010, doi: 10.1115/1.4027681.
22. K. VijayaSekhar, SanghamitraDebroy, V. Pavan Kumar Miriyala, Swati Ghosh Acharyya, and Amit Acharyya, Self-healing phenomena of graphene: potential and applications, *Open Phys.* 14, (2016), 364, <https://doi.org/10.1515/phys-2016-0040>.
23. B. Zhang, L. Mei and H. F. Xiao, Nanofracture in graphene under complex mechanical stresses, *Appl. Phys. Lett.*, 101(12), (2012), 121915, doi: <http://dx.doi.org/10.1063/1.4754115>.
24. Y.Y. Zhang, C.M. Wang, Y. Cheng and Y. Xiang, Mechanical properties of bilayer graphene sheets coupled by sp^3 bonding, *Carbon*, 49 (2011), 4511, <http://dx.doi.org/10.1016/j.carbon.2011.06.058>.
25. L. Wang and Q. Zhang, Elastic behavior of bilayer graphene under in-plane loadings, *Curr. Appl. Phys.* 12, (2012), 1173-1177, <http://dx.doi.org/10.1016/j.cap.2012.02.043>.
26. SanghamitraDebroy, V. Pavan Kumar Miriyala, K. VijayaSekhar, Swati GhoshAcharyya and AmitAcharyya, Self healing nature of bilayer graphene, *Superlattices and Microstructures*, 96, (2016), 26-35, <http://dx.doi.org/10.1016/j.spmi.2016.05.010>
27. A. Hashimoto, K. Suenaga, A. Gloter, K. Urita and S. Iijima, Direct evidence for atomic defects in graphene layers, *Nature*, 430, (2004), 870, DOI:10.1038/nature02817.
28. J. Coraux, A. T. N. 'Diaye, C. Busse, and T. Michely, Structural Coherency of Graphene on Ir(111), *Nano Lett.*, 8 (2), (2008), 565, DOI: 10.1021/nl0728874
29. M. A. Rafiee, J. Rafiee, I. Srivastava, Z. Wang, H. Song, Z. Z. Yu et.al., Fracture and fatigue in graphene nanocomposites, *Small* 6(2), (2010), 179, doi: 10.1002/sml.200901480.
30. A. Zandiatashbar, G. H. Lee, S. J. An, S. Lee, N. Mathew, M. Terrones et.al., Effect of defects on the intrinsic strength and stiffness of graphene, *Nature Communications* 5, (2014), 3186, doi: 10.1038/ncomms4186.
31. K. Verguts, N. Vrancken, B. F. Vermeulen, C. Huyghebaert, H. Terryn, S. Brems et.al., Single-Layer Graphene Synthesis on a $Al_2O_3(0001)/Cu(111)$ Template Using Chemical Vapor Deposition, *ECS Journal of Solid State Science and Technology*, 5 (11), (2016), Q3060-Q3066, doi: 10.1149/2.0121611jss.
32. W. Liu, H. Li, C. Xu, Y. Khatami, K. Banerjee, Synthesis of high-quality monolayer and bilayer graphene on copper using chemical vapor deposition, *CARBON*, 49, (2011), 4122 – 4130, <http://doi.org/10.1016/j.carbon.2011.05.047>.

33. A. Reina, X. Jia, J. Ho, D. Nezich, H. Son, V. Bulovic et.al., Large Area, Few-Layer Graphene Films on Arbitrary Substrates by Chemical Vapor Deposition, *Nano Lett.*, 9 (1), (2009), pp 30–35, DOI: 10.1021/nl801827v.
34. A. W. Robertson and J. H. Warner, Hexagonal Single Crystal Domains of Few-Layer Graphene on Copper Foils, *Nano Lett.*, 11 (3), (2011), pp 1182–1189, DOI: 10.1021/nl104142k
35. Yu Q, Jauregui LA, Wu W, Colby R, Tian J, Su Z, et al, Control and characterization of individual grains and grain boundaries in graphene grown by chemical vapour deposition, *Nat Mater*, 10 (6), (2011) pp 443-449, doi:10.1038/nmat3010
36. Huang PY, Ruiz-Vargas CS, van der Zande AM, Whitney WS, Levendorf MP, Kevek JW, et al, Grains and grain boundaries in single-layer graphene atomic patchwork quilts, *Nature*, ; 469 (7330), (2011),pp 389-392, doi:10.1038/nature09718
37. Li X, Magnuson CW, Venugopal A, Tromp RM, Hannon JB, Vogel EM, et al, Large-Area Graphene Single Crystals Grown by Low-Pressure Chemical Vapor Deposition of Methane on Copper. *Journal of the American Chemical Society* 2011; 133 (9): 2816-2819
38. Yan Z, Lin J, Peng Z, Sun Z, Zhu Y, Li L, et al. Toward the Synthesis of Wafer-Scale Single-Crystal Graphene on Copper Foils. *ACS Nano* 2012; 6 (10): 9110-9117.
39. Chen S, Ji H, Chou H, Li Q, Li H, Suk JW, et al. Millimeter-Size Single-Crystal Graphene by Suppressing Evaporative Loss of Cu During Low Pressure Chemical Vapor Deposition. *Advanced Materials* 2013; 25 (14): 2062-2065.
40. Mohsin A, Liu L, Liu P, Deng W, Ivanov IN, Li G, et al. Synthesis of Millimeter-Size Hexagon-Shaped Graphene Single Crystals on Resolidified Copper. *ACS Nano* 2013; 7 (10): 8924-8931.
41. Zhou H, Yu WJ, Liu L, Cheng R, Chen Y, Huang X, et al. Chemical vapour deposition growth of large single crystals of monolayer and bilayer graphene. *Nat Commun* 2013; 4, 2096.
42. Gan L, Luo Z, Turning off Hydrogen To Realize Seeded Growth of Subcentimeter Single-Crystal Graphene Grains on Copper. *ACS Nano* 2013; 7 (10): 9480-9488.
43. Hao Y, Bharathi MS, Wang L, Liu Y, Chen H, Nie S, et al. The Role of Surface Oxygen in the Growth of Large Single-Crystal Graphene on Copper. *Science* 2013; 342 (6159): 720-723.
44. A. W. Cummings , D. L. Duong , V. L. Nguyen , D. V. Tuan , J. Kotakoski , J. E. B. Vargas , Y. H. Lee , S. Roche. Controlling Defects in Graphene for Optimizing the Electrical Properties of Graphene Nanodevices. *Adv. Mater.* 2014 ,26 , 5079
45. Dechao Geng , Huaping Wang , and Gui Yu, Graphene Single Crystals: Size and Morphology Engineering. *Adv Mater.* 2015; 27(18): 2821-37.
46. S. Plimpton, Fast Parallel Algorithms for Short-Range Molecular Dynamics, *J. Comp. Phys.* 117 (1995) 1-19, <http://dx.doi.org/10.1006/jcph.1995.1039>.
47. S. J. Stuart, A. B. Tutein and J. A. Harrison, A reactive potential for hydrocarbons with intermolecular interactions, *J. Chem. Phys.*, 112(14), (2000), 6472, doi: <http://dx.doi.org/10.1063/1.481208>.
48. R. Faccio, P. A. Denis, H. Pardo, C. Goyenola and A. W. Momburu, Mechanical properties of graphene nanoribbons, *J. Phys.: Condens. Matter* 21, (2009), 285304, doi:10.1088/0953-8984/21/28/285304

49. O. A. Shenderova, D. W. Brenner, A. Omeltchenko, X. Su, and L. H. Yang, Atomistic modeling of the fracture of polycrystalline diamond, *Phys. Rev. B* 61, (2000), 3877, DOI: <https://doi.org/10.1103/PhysRevB.61.3877>.
50. J.E. Lennard-Jones, On the Determination of Molecular Fields. I. From the Variation of the Viscosity of a Gas with Temperature, *Proc. Roy. Soc. Lond. A* 106, (1924), 441-462, <http://dx.doi.org/10.1098/rspa.1924.0081>.
51. W. Tao, G. Qing, L. Yan and S. Kuang, A comparative investigation of an AB- and AA-stacked bilayer graphene sheet under an applied electric field: A density functional theory study, *Chin. Phys. B* Vol. 21, No. 6, (2012), 067301, DOI: 10.1088/1674-1056/21/6/067301.
52. P. Hofmann, Bilayer graphene: A little twist with big consequences, *NATURE MATERIALS*, 12, (2013), 874, doi:10.1038/nmat3764.
53. J. Zhu, M. He, and F. Qiu, Effect of Vacancy Defects on the Young's Modulus and Fracture Strength of Graphene: A Molecular Dynamics Study, *Chin. J. Chem.* 30(7), (2012), 1399–1404, <https://doi.org/10.1002/cjoc.201200505>
54. M. C. Wang, C. Yan, L. Ma and N. Hu, Molecular dynamics investigation on edge stress and shape transition in graphenenanoribbons, *Comput. Mater. Sci.* 68, (2013), 138, <http://dx.doi.org/10.1016/j.commatsci.2012.09.035>
55. Y. Zheng, N. Wei, Z. Fan, L. Xu and Z. Huang, Mechanical properties of grafold: a demonstration of strengthened graphene, *Nanotechnology* 22, (2011), 405701, <http://dx.doi.org/10.1088/0957-4484/22/47/479501>.
56. Dumitrica, M. Hua, B.I. Yakobson, Symmetry-, time-, and temperature-dependent strength of carbon nanotubes, *Proc. Natl. Acad. Sci. U.S.A.* 103 (16), (2006), 6105-6109, <http://dx.doi.org/10.1073/pnas.0600945103>.

Highlights

- Strength of pristine single layer graphene at 1073 K is 4% higher for armchair direction and 6.4 % for zigzag direction compared to bilayer AA stacked armchair graphene.
- The presence of a vacancy reduces the strength of single layer graphene sheet by 15 ± 5 % and bilayer graphene by 17 ± 8 % at 300 K.
- Strength of single and bilayer graphene falls by ~ 30 % on increasing temperature to 1073 K and in presence of vacancy.
- AB stacked graphene has two-step fracture. The sheet having armchair orientation fails first followed by zigzag.
- The ultimate tensile strength of AB graphene at 1073 K is 22% less than at 300 K.